# Control of Afterbody Vortices by Blowing

R. Jackson*, Z.Wang† and I. Gursul‡
*Department of Mechanical Engineering, University of Bath, Bath, BA2 7AY, UK*

**An experimental study has been performed to examine the effect of blowing via a pair of jets from the upswept face of a slanted base cylinder, upon the development of the afterbody vortex flow field. Jet vortices initially interact with the shear layer separated from the upswept section. The nature of the early interactions between the jet and shear layer is highly dependent upon the blowing direction. For most blowing configurations tested, the shear layer becomes wrapped around the jet vortex. The most significant evidence of modification of the afterbody vortex pair was found when initiating a jet vortex further outboard and closer to the shear layer. The jet/vortex interactions initially cause the afterbody vortices to form further outboard, at a greater distance from the surface, and with a smaller vortex core. There is a reduction in the circulation over the first half of the afterbody length, before it recovers to baseline levels at the trailing edge. The vortex pair appears more diffuse near the trailing edge, but this is a result of increased meandering.**

## Nomenclature

| | | | | | |
|---|---|---|---|---|---|
| $a_m$ | = | meandering amplitude | $x_j$ | = | streamwise jet location |
| $A_j$ | = | cross-sectional area of jet | $y$ | = | normal distance |
| $c$ | = | chord length of upswept face | $z$ | = | spanwise distance |
| $C_\mu$ | = | jet momentum coefficient, $\rho A_j U_j^2/0.5\rho U_\infty^2 S$ | $z_j$ | = | spanwise jet location |
| $D$ | = | diameter of fuselage | $\alpha$ | = | fuselage incidence angle |
| $L$ | = | length of afterbody | $\alpha_j$ | = | jet incidence angle |
| $r$ | = | distance from vortex center | $\beta$ | = | fuselage yaw angle |
| $Re$ | = | Reynolds number, $\rho U_\infty D/\mu$ | $\beta_j$ | = | jet yaw angle |
| $S$ | = | cross-sectional area of fuselage | $\Gamma$ | = | circulation |
| $U_j$ | = | jet velocity | $\mu$ | = | viscosity |
| $U_\infty$ | = | freestream velocity | $\rho$ | = | density |
| $V$ | = | crossflow velocity | $\omega$ | = | vorticity |
| $x$ | = | streamwise distance | | | |

## I. Introduction

To facilitate the rear loading and removal of cargo, the afterbodies of military transport aircraft exhibit a high angle of upsweep. This angle is the cause of a large region of low pressure in the near-wake, resulting in the formation of a longitudinal counter-rotating vortex pair which is convected downstream.[1,2]

Force measurements on geometries with an axisymmetric forebody and a slanted base have shown that the drag coefficient increases with upsweep angle for a given Reynolds number.[3,4] This evidence demonstrates why the issue is more pertinent to military transport aircraft compared to their civil counterparts. Alongside an increase in drag coefficient, the vortex pair can disrupt the trajectory of objects during airdrop missions. Controlling the formation of these vortices could result in an increased mission range, fuel cost savings to the operator, and a higher mission success rate.

A range of vortex control mechanisms have been developed over the past few decades to varying degrees of success. In the 1960s, the first example of afterbody drag reduction was installed on the Short Belfast.[5] Aft fuselage

* Postgraduate Research Student, Dept. of Mechanical Engineering, Student Member AIAA.
† Lecturer, Dept. of Mechanical Engineering.
‡ Professor of Aerospace Engineering, Dept. of Mechanical Engineering, Associate Fellow AIAA.

mounted strakes were designed to reduce inflow to the upswept region, modifying the formation and location of the vortex pair. More recent studies into the efficacy of different designs of passive vortex generators have shown promising drag reduction results.[6-8] In these solutions, the passing of air over arrays of small strakes generates additional vortices that may interact with the afterbody vortices. However, in some instances, these passive flow control designs can create operational difficulties during airdrop missions and the loading/unloading of cargo.[8]

A gap in the existing research has been identified within the application of blowing techniques to the afterbody vortex problem. Previous research has shown that there is potential for rapid diffusion of wing tip vortices in the near-wake by means of ingestion of jet turbulence from continuous jets.[9,10] The interaction of jet vortices with wing tip vortices can also cause them to become more diffuse, but the result is highly dependent on jet location, blowing direction and jet momentum coefficient, $C_\mu$. These jet vortices have previously been generated through: a) blowing at an angle to the freestream direction;[11] b) self-generated jets (bleed) ejected perpendicular to the wing surface, where the pressure differential between the two wing surfaces provides the input energy;[12] and c) synthetic jets.[13] There is also evidence that far-wake interactions of co-rotating and counter-rotating vortex pairs can be affected by turbulence ingestion from blowing.[14-16] It has been theoretically shown that three-dimensional instabilities may grow in a counter-rotating vortex pair.[17]

The aims of this experimental study are to investigate the interactions between a pair of jets, emanating from the upswept face of a simplified fuselage model, and the afterbody vortex pair, and to understand how these interactions are affected by the blowing location and direction. This is compared against the baseline flow field (without blowing). The flow field was captured using 2D Particle Image Velocimetry (PIV) in a water tunnel. The effect of changing the pitch and yaw angle of the model is also presented.

## II. Experimental Methods

### A. Model Design

In order to separate the secondary flow effects influenced by the main wing and empennage from that of the afterbody section, the fuselage model is reduced to a slanted base axisymmetric cylinder. The afterbody has a constant upsweep angle of 28°, similar to that on a Lockheed Martin C-130 'Hercules'. The face of the upsweep is assumed to be flat. The cylindrical midbody is connected to an ellipsoidal nose. The fuselage diameter is 88.9 mm and is scaled at 1:47.2 to that of the C-130. The total length of the model is 456 mm. The geometry of the model, in reference with the main axes and dimensions, is presented in Fig. 1.

The midbody of the model is manufactured from a section of ABS pipe, with the nose printed from ABS plastic. The afterbody section is molded out of Glass fiber Reinforced Plastic. The afterbody contains an inlet to a small plenum chamber just behind the upswept face, through which water is expelled for the blowing case. Energy to generate the blowing jets is supplied to the plenum chamber by air pressurized at 1 bar. The jet flow rate is controlled by a variable area flowmeter. The model is mounted on a fairing with a NACA 0012 airfoil cross-section, which also houses the water delivery system for the blowing case.

### B. Experimental Setup

Experiments were performed in a free-surface, closed-loop water tunnel (Eidetics Model 1520) within the Department of Mechanical Engineering at the University of Bath. The working test area has an internal cross-section of 381 mm x 508 mm, and a length of 1530 mm. The maximum flow velocity is 0.5 m/s, and the freestream turbulence intensity is approximately 0.5%. The Reynolds number was kept constant at Re = 20,000 (based on fuselage diameter), giving a freestream velocity of around $U_\infty$ = 0.25 m/s. This is significantly less than the Reynolds numbers experienced in flight for the C-130, but fortunately, during their investigations, Epstein et al. noted that the "shape of the vortices did not seem to be a function of the test Reynolds number", and that "no clear dependence on Reynolds number was observed in the results".[2] The estimated uncertainty for velocity measurements is ±1.5%.

PIV images were captured using a 200 mm f/2.8D lens attached to a Powerview Plus 12-bit digital CCD camera with a resolution of 3,312 x 2,488 pixels. The seeding particles used were hollow glass spheres with diameters in the range of 8 µm to 12 µm. These were illuminated using a 200 mJ dual Nd:YAG pulsed laser, which generated a laser sheet of approximately 1 mm thickness. The timings of both devices were controlled via a TSI Model 610034 synchronizer connected to a PC. Figure 2 illustrates the setup of the equipment. Crossflow velocity measurements were taken at five stations over the afterbody section (x/L = {0.2, 0.4, 0.6, 0.8, 1.0}), with the laser positioned from the side, generating a sheet perpendicular to the freestream. The Hart cross-correlation algorithm was used to process the images, with an interrogation window of 32 x 32 pixels and a 50% overlap, giving a spatial resolution in

the range of 0.7 mm to 0.9 mm, or approximately 1% of the fuselage diameter. Time-averaged data was calculated from 300 pairs of images.

### C. Selection of Parameters for Blowing

A pair of circular holes of 1 mm diameter positioned symmetrically either side of the fuselage centerline provided the path through which the jets exited. The main parameters that were varied were the streamwise location of the blowing jets ($x_j/L$), and the jet incidence ($\alpha_j$) and yaw angles ($\beta_j$). Six different configurations were tested, as outlined in Table 1. The two streamwise locations tested were $x_j/L = 0.12$ and $x_j/L = 0.20$. Preliminary flow visualization results indicated that blowing at locations further downstream than $x_j/L = 0.20$ had little effect upon the afterbody vortices, and are therefore not presented in this paper. In the spanwise direction, the jet is located at $z_j/D = \pm 0.146$ for $x_j/L = 0.12$ and $z_j/D = \pm 0.240$ for $x_j/L = 0.20$. Figure 3a demonstrates how the jets located at $x_j/L = 0.12$ are positioned in relation to the trajectory of the afterbody vortices in the baseline case.

The jet incidence angle was tested at $\alpha_j = 30°$ and $\alpha_j = 90°$. This angle is defined in Fig. 3b. The lower incidence angle is limited by the thickness of the plate (3 mm) through which the jets are expelled, as well as the length of the local span. Blowing perpendicular to the surface at $\alpha_j = 90°$ enables later comparisons with some studies into the control of wing tip vortices.[11,12]

To allow easy adjustment of the yaw angle, the jet holes were cut out of thin discs of 15 mm diameter, which could then be rotated in-situ. The jet yaw angle was tested at $\beta_j = 0°$ and $\beta_j = 90°$. Blowing outboard where $\alpha_j = 30°$ and $\beta_j = 0°$ is expected to disrupt the shear layer and vortex formation, while the jet formed from blowing at $\alpha_j = 30°$, $\beta_j = 90°$ should be almost parallel to the freestream direction (with a theoretical offset of 2°). However, unlike the studies by Phillips and Graham[9] and Margaris et al.[10], the presence of the vortex pair produces an upwash, which ensures that the local velocity around the vortices is not in the same direction as the freestream. The uncertainty in the jet angles is estimated to be ±2°.

The jet momentum coefficient adopted for all blowing configurations was $C_\mu = 0.02$, giving a jet velocity of around $U_j = 1.6$ m/s; but a study into its influence is planned for the future. This value of $C_\mu$ is comparable to other flow control studies.[15]

**Table 1. The blowing configurations tested.**

| No. | $x_j/L$ | $z_j/D$ | $\alpha_j$ | $\beta_j$ |
|---|---|---|---|---|
| 1 | 0.12 | ±0.146 | 30° | 0° |
| 2 | 0.12 | ±0.146 | 30° | 90° |
| 3 | 0.12 | ±0.146 | 90° | N/A |
| 4 | 0.20 | ±0.240 | 30° | 0° |
| 5 | 0.20 | ±0.240 | 30° | 90° |
| 6 | 0.20 | ±0.240 | 90° | N/A |

## III. Results and Discussion

### A. Baseline Flow Field

The baseline case is characterized with the model at $\alpha = 0°$ and $\beta = 0°$. Figure 4 presents the time-averaged crossflow vorticity and the progression of the vortex pair as it travels downstream. At the furthest forward station of $x/L = 0.2$ (Fig. 4a), a shear layer develops and feeds vortical flow downwards from either side of the upsweep edge inboard to where a condensed counter-rotating vortex pair forms. The streamline plots in Fig. 5 indicate the development of the flow field. As the vortices convect downstream, the upwash generated by the counter-rotation (demonstrated in Fig. 5) displaces them vertically, so that they initially follow the contour of the upswept face.

Between $x/L = 0.2$ and $x/L = 0.6$ (Fig. 4a to Fig. 4c), the vortices grow substantially, becoming elliptical in shape. They experience a simultaneous displacement outboard as they appear to roll-up back over the shear layer. Small pockets of flow recirculating in the opposite direction are present in the enclosed region between the vortices and shear layer. These are due to the secondary vortices produced by the flow separation on the surface. At $x/L = 0.6$, the vortex pair have become more circular and slightly diffuse. The shear layer also appears to have weakened. The narrowing of the afterbody span beyond $x/L = 0.5$ may have an effect upon the strength of the shear layer. The pressure differential between the freestream and upsweep region has been shown to reduce with streamwise distance, albeit for a slightly different geometry.[2] Hence, the driving mechanism behind shear layer formation loses impetus.

As the spanwise separation of the vortex pair increases, the influence of one upon the other lessens, such that the vertical displacement between each station reduces. This causes the pair to move away from the surface between x/L = 0.6 and x/L = 0.8 (Fig. 4d). Examining the streamline density indicates that the region of largest velocity magnitude shifts towards the centerline with increasing streamwise distance. At x/L = 1.0 (Fig. 4e), the vortices are at their most circular, and remain almost symmetric about the y axis.

Figure 6 summarizes the change in strength of the vortex pair with streamwise distance. The circulation is determined from the area integral of vorticity. Initially, the center of each vortex is found. In this study, vortices are identified as regions where the application of the Q Criterion returns values of $Q > 0$.[18] For each crossflow measurement plane, the center of each vortex is defined as the location with maximum Q. This method ensures that the vorticity contribution from the wall shear layer is not taken into account when finding the vortex center, as in some instances the maximum vorticity is located within the shear layer. It is more appropriate to apply this method to asymmetric vortices, such as those identified in this study, than using the minimum velocity approach, as the location of maximum vorticity is not necessarily coincident with that of the center of rotation. Once the vortex center is identified, the circulation of this center is then calculated, before expanding out by one spatial resolution unit at a time and recalculating the circulation, until the change between iterations is less than 1%.

The increase in circulation with streamwise distance is initially rapid, before slowing after x/L = 0.6, as shown in Fig. 6. Approximately 90% of the vortex circulation at x/L = 1.0 has already been reached by x/L = 0.6. This agrees well with the idea that growth is dependent upon the strength of the shear layer. Some slight asymmetry is present between the two vortices, possibly due to uncertainties in yaw (approximately ±0.5°), or geometric irregularities with the model.

### B. Non-zero Fuselage Pitch and Yaw

Figure 7 compares variations in the baseline flow field at x/L = 1.0 (Fig. 7a) with two fuselage incidence angles of $\alpha = -2°$ and $\alpha = +2°$, which encompasses the typical range experienced during the majority of a mission. At a negative $\alpha$ (Fig. 7b), the effective angle that the upsweep creates with the freestream is increased. Because of this, the vortex pair have gained in strength, with the average circulation of both vortices increasing by 15%, as summarized in Table 2. The size and shape of the core region remains similar to the baseline case. The position of the vortices appears to have been displaced downwards, but this is a result of the angle that the camera creates with the fuselage centerline. With the fuselage at a positive $\alpha$ (Fig. 7c), the vortex pair is weaker, and appears more diffuse, with the average circulation of the two vortices reducing by 13%. The flow field implications of a yaw angle of $\beta = 2°$ are shown in Fig. 7d, which simulates the scenario of a crosswind. A non-zero yaw angle promotes an unequal strength vortex pair. The right vortex (closest to the starboard side, which has become more exposed to the freestream) becomes the more dominant of the two, highlighted by a discrepancy of 12% in the circulation when compared to the weaker, left vortex. The shape of both vortex cores has also become less coherent.

**Table 2. Effect of a non-zero pitch or yaw angle upon the circulation at x/L = 1.0.**

| $\alpha$ | $\beta$ | $\lvert\Gamma\rvert/cU_\infty$ (Left vortex) | $\lvert\Gamma\rvert/cU_\infty$ (Right vortex) |
|---|---|---|---|
| 0° | 0° | 0.234 | 0.229 |
| -2° | 0° | 0.275 | 0.258 |
| +2° | 0° | 0.210 | 0.194 |
| 0° | +2° | 0.223 | 0.251 |

### C. Effect of Jet Orientation

The early stage interactions between the afterbody vortex pair and blowing jets are presented in Fig. 8, specifically when blowing from the furthest upstream of the two streamwise locations, $x_j/L = 0.12$. These different crossflow vortex structures depicted at x/L = 0.2 are compared against the baseline case in Fig. 8a. Blowing perpendicular to the surface ($\alpha_j = 90°$) introduces a region of vorticity, opposite in sign to the respective afterbody vortex (Fig. 8b), which then interacts with the shear layer. This pulls the tip of the shear layer downward, reducing the magnitude of the developing afterbody vortex. The shear layer extends spanwise towards the fuselage centerline by a comparable distance to that of the baseline case.

Blowing in an outboard direction (Fig. 8c) produces a more defined counter-rotating jet vortex, which is closer to the shear layer and further outboard. The jet vortex wraps the shear layer around it, shortening the distance by which it extends towards the fuselage centerline. The strength and thickness of the shear layer has increased, and it is forced closer to the upswept surface.

Jets exiting from the surface at an angle of $\alpha_j = 30°$ and $\beta_j = 90°$ (Fig. 8d) form smaller vortices near to the surface. The shear layer appears to be wrapped around the jet vortex, causing the afterbody vortex core to shift further outboard along the spanwise direction. Similarly with Fig. 8c, the strength of the shear layer has increased.

The flow field of one of the more promising blowing configurations ($x_j/L = 0.2$ $\alpha_j = 30°$ and $\beta_j = 0°$) is presented alongside the baseline case in Fig. 9. At x/L = 0.2 (Fig. 9a), the shear layer has intensified but retracted. The splitting of the shear layer by the jet is also apparent. Further downstream at x/L = 0.4 (Fig 9b), the core size of the afterbody vortices has reduced, and become more circular, while the separation distance of the vortex centers has increased. The faint features of the interaction of the afterbody vortex with the jet vortex are still noticeable. It is expected that the vortex interactions slightly upstream of this plane to be similar in nature to those in Fig. 8c. At x/L = 0.6 (Fig. 9c), the vortices have displaced further from the surface when compared to the baseline, with the continuing trend of a reduced vortex core size. At the final two measurement planes (Fig. 9d and Fig. 9e), the vortices appear more diffuse.

The effect of the six different blowing configurations upon the circulation is presented in Fig. 10. Evidence suggests that blowing at $x_j/L = 0.12$ (Fig. 10a to Fig. 10c), results in a stronger afterbody vortex pair at the first crossflow station, compared to blowing at $x_j/L = 0.2$ (Fig. 10d to Fig. 10f). Aside from this, the trends between the two blowing streamwise locations, for a given jet configuration, are similar. The most noticeable deviation from the baseline case is seen when blowing with a jet direction of $\alpha_j = 30°$, $\beta_j = 0°$ (Fig. 10a and Fig. 10d). Although the afterbody vortex pair is stronger at x/L = 0.2 in Fig. 10a, the growth decelerates substantially following x/L = 0.4, so much so that the discrepancy with the baseline case is greater than 10% at x/L = 0.6. The same is true for Fig. 10d. The decrease in the circulation at x/L = 0.6 appears to be due to the smaller vortex core size (see Fig. 9c). However, the vortex pair recover and return to a circulation close to that of the baseline at the afterbody trailing edge. The benefits of blowing at $\alpha_j = 30°$, $\beta_j = 90°$ are less noticeable (Fig. 10b and Fig. 10e), but the maximum deviation from the baseline circulation still appears to occur at x/L = 0.6. Figure 10c and Fig. 10f suggest that blowing perpendicular to the surface is not as effective as observed in previous studies[12], possibly because the jet vortex forms too far from the surface for the vortex interactions (Fig. 8b) to be efficient at diffusing the afterbody vortex.

**D. Vortex Meandering**

The variation of afterbody vortex meandering amplitude ($a_m$), as a function of streamwise distance, is shown in Fig. 11 for the baseline case and the blowing configuration, where $x_j/L = 0.2$, $\alpha_j = 30°$, $\beta_j = 0°$. The meandering amplitude is defined as:

$$a_m = \left( \frac{1}{N} \sum_{i=1}^{i=N} (z_i - z_c)^2 + (y_i - y_c)^2 \right)^{1/2} \tag{1}$$

where N is the number of PIV snapshots, $z_i$ and $z_c$ are the center coordinates of the instantaneous and time-averaged vortex in the spanwise direction, $y_i$ and $y_c$ are the center coordinates of the instantaneous and time-averaged vortex in the normal direction. Figure 11 demonstrates a general increase of meandering amplitude with streamwise distance up to x/L = 0.8, beyond which a decrease occurs. The variation in the shape of the baseline and blowing curves are similar, aside from deviations at the furthest upstream station, where the dominance of the shear layer creates difficulty in defining the center of the developing vortex. There is a slight increase in the meandering amplitude at x/L = 0.8 and x/L= 1.0 with blowing. This may be a contributing factor to the more diffuse time-averaged vortex seen in Fig. 9e.

In order to understand the effects of blowing upon the instantaneous vortex, crossflow vorticity profiles of the vortex pair at x/L = 1.0 are presented in Fig. 12. This shows the time-averaged profile, as well as the mean of all instantaneous profiles. For both vortices, the magnitude of the time-averaged and instantaneous vorticity in the blowing case is less than the baseline. There is a more significant reduction of 18% in the maximum mean vorticity compared to an 11% reduction in the maximum instantaneous vorticity. The circulation at x/L = 1.0 is very similar to the baseline, as seen in Fig. 10d, suggesting that the more diffuse structure of the time-averaged vortex is due to the increased meandering.

The correlation coefficient between the y and z locations of the vortex pair centers was found to be consistently less than 0.2, with no noticeable change with the streamwise location of the crossflow measurement plane. This indicates that the influence of one vortex upon the other is small, probably because the separation distance is too large.

## IV. Conclusions

In this paper, properties of the flow field in the near-wake of an axisymmetric slanted base cylinder, with and without blowing, have been presented. PIV measurements provided additional insight into the formation of the afterbody vortex pair for the baseline case, indicating that the majority of vortex growth, and circulation increase, occurs before x/L = 0.6. This is while the shear layers are at their strongest and feeding vorticity into the vortex pair. The measurements revealed the trajectory of the vortices as they are convected downstream. They initially form close to the surface before moving away, and transition from elliptic through to circular in structure.

Positioning the model at a non-zero pitch or yaw angle did not significantly affect the structure of the afterbody vortices seen at x/L = 1.0. However, the circulation was shown to increase when the fuselage was set at a negative pitch angle, as the effective angle between the upsweep and freestream is increased. The opposite was demonstrated at a positive pitch angle. A non-zero yaw angle produces a vortex pair with unequal strengths.

The direction at which the blowing jets emanate from the upswept face is influential upon the early vortex/jet interaction, more so than the streamwise locations investigated. Out of the configurations tested, results suggest that initiating jet vortices further outboard and closer to the shear layer is the most effective at modifying the afterbody vortex pair. In this instance, the vortices form more outboard and further away from the surface during their initial development. These features may help in reducing the afterbody drag. Although there was some decrease in the circulation, the difference becomes negligible towards the trailing-edge of the afterbody. The vortices seen at the last two crossflow stations appear more diffuse, but this is due to the increased meandering.

Further work to be performed includes: undertaking force measurements and volumetric measurements; investigating the influence of the spanwise blowing location, blowing coefficient $C_\mu$ and the number of blowing jets; and assessing the efficacy of other methods of jet generation, such as synthetic, bleed or pulsed.

## Acknowledgements

This research is sponsored by the AFOSR, under the grant number FA9550-14-1-0126.

## References

[1]Bury, Y., Jardin, T. and Klockner, A., "Experimental Investigation of the Vortical Activity in the Close Wake of a Simplified Military Transport Aircraft," *Experiments in Fluids*, Vol. 54, No. 5, 2013, pp. 1-15.

[2]Epstein, R. J., Carbonaro, M. C., and Caudron, F., "Experimental Investigation of the Flowfield About an Upswept Afterbody," *Journal of Aircraft,* Vol. 31, No. 6, 1994, pp. 1281-1290.

[3]Bearman, P. W., "Bluff Body Flows Applicable to Vehicle Aerodynamics," *Journal of Fluids Engineering,* Vol. 102, No. 3, 1980, pp. 265-274.

[4]Britcher, C. P., and Alcorn, C. W., "Interference-Free Measurements of the Subsonic Aerodynamics of Slanted-Base Ogive Cylinders," *AIAA Journal,* Vol. 29, No. 4, 1991, pp. 520-525.

[5]McCluney, B. and Marshall, J., "Drag Development of the Belfast," *Aircraft Engineering and Aerospace Technology,* Vol. 39, No. 10, 1967, pp. 33-37.

[6]Calarese, W., Crisler, W. P., and Gustafson, G. L., "Afterbody Drag Reduction by Vortex Generators," *AIAA 23rd Aerospace Sciences Meeting,* AIAA, New York, NY, 1985.

[7]Wortman, A., "Reduction of Fuselage Form Drag by Vortex Flows," *Journal of Aircraft,* Vol. 36, No. 3, 1999, pp. 501-506.

[8]Smith, B. R., Yagle, P. J. and Hooker, J. R., "Reduction of Aft Fuselage Drag on the C-130 Using Microvanes," *AIAA 51st Aerospace Sciences Meeting,* AIAA, Reston, VA, 2013.

[9]Phillips, W. R. C., and Graham, J. A. H., "Reynolds-Stress Measurements in a Turbulent Trailing Vortex," *Journal of Fluid Mechanics,* Vol. 147, Oct., 1984, pp. 353-371.

[10]Margaris, P., Marles, D., and Gursul, I., "Experiments on Jet/Vortex Interaction," *Experiments in Fluids,* Vol. 44, No. 2, 2008, pp. 261-278.

[11]Margaris, P., and Gursul, I., "Vortex Topology of Wing Tip Blowing," *Aerospace Science and Technology,* Vol. 14, No. 3, 2010, pp. 143-160.

[12]Hu, T., Wang, Z., and Gursul, I., "Passive Control of Roll Oscillations of Low-aspect-ratio Wings Using Bleed," *Experiments in Fluids,* Vol. 55, No. 6, 2014, pp. 1-16.

[13]Margaris, P., and Gursul, I., "Wing Tip Vortex Control Using Synthetic Jets," *The Aeronautical Journal,* Vol. 110, No. 1112, 2006, pp. 673-681.

[14]Bearman, P., Heyes, A., Lear, C., and Smith, D., "Natural and Forced Evolution of a Counter Rotating Vortex Pair," *Experiments in Fluids,* Vol. 40, No. 1, 2006, pp. 98-105.

[15]Marles, D., and Gursul, I., "Effect of an Axial Jet on Vortex Merging," *Physics of Fluids,* Vol. 20, No. 4, 2008, pp. 1-16.

[16]Marles, D., "Effect of an Axial Jet on Aircraft Wake Vortices," Ph.D. Thesis, University of Bath, UK, 2008.

[17]Donnadieu, C., Sabine, O., Chomaz, J., and Billant, P., "Three-dimensional Instabilities and Transient Growth of a Counter-rotating Vortex Pair," *Physics of Fluids,* Vol. 21, No. 9, 2009, pp. 1-16.

[18]Jeong, J. and Hussain, F., "On the Identification of a Vortex," *Journal of Fluid Mechanics,* Vol. 285, Feb., 1995, pp. 69-94.

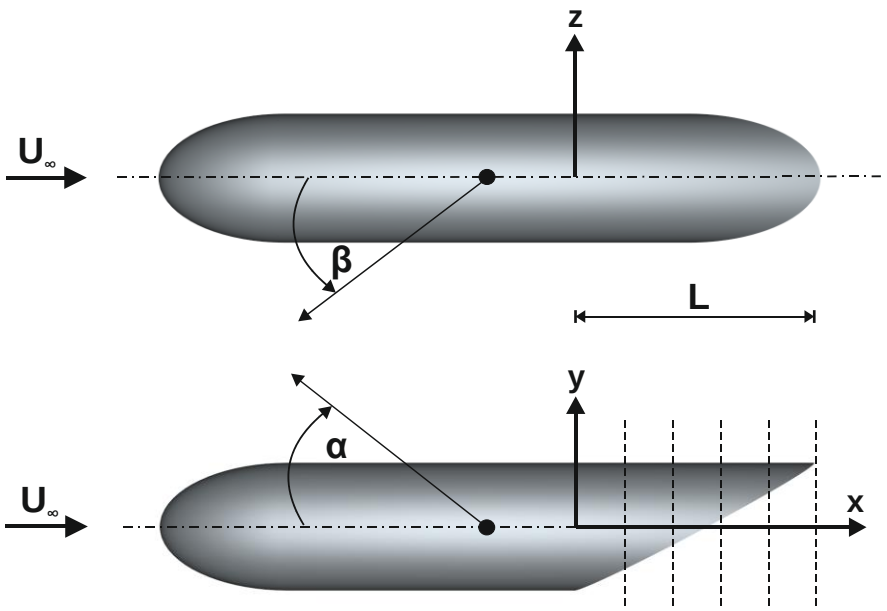


**Figure 1. Outline of the simplified fuselage model showing top-down (above) and side view (below). Crossflow measurement planes are indicated on the side view by dashed lines.**

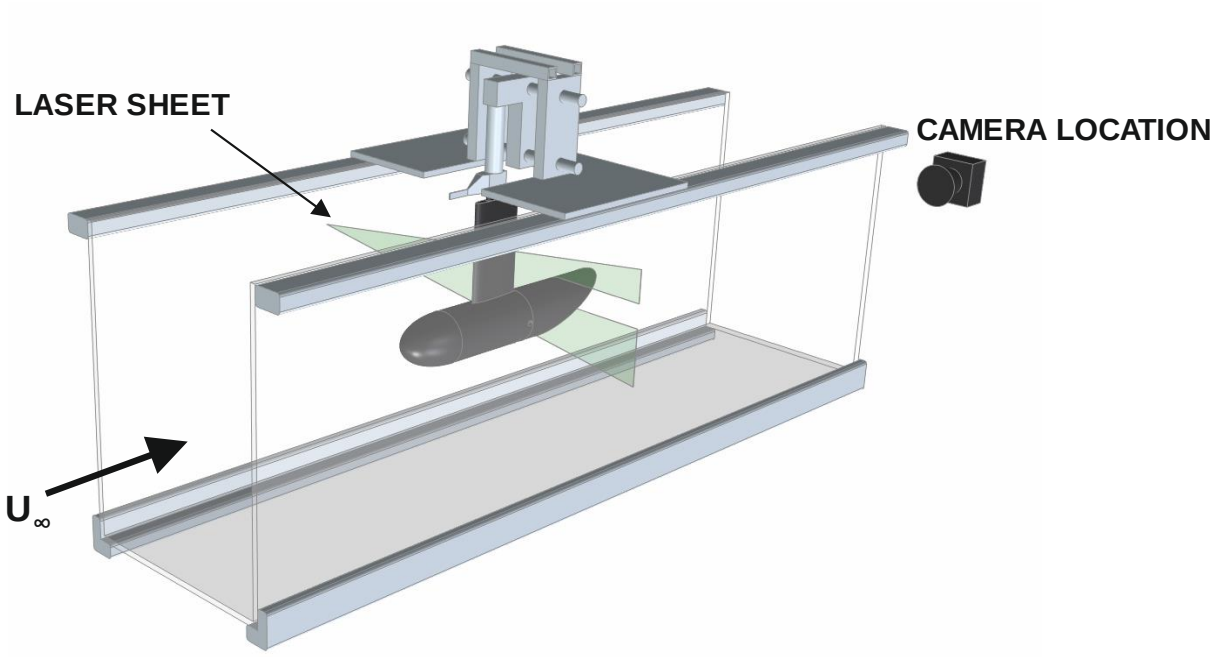


**Figure 2. Schematic of the experimental setup in the water tunnel.**

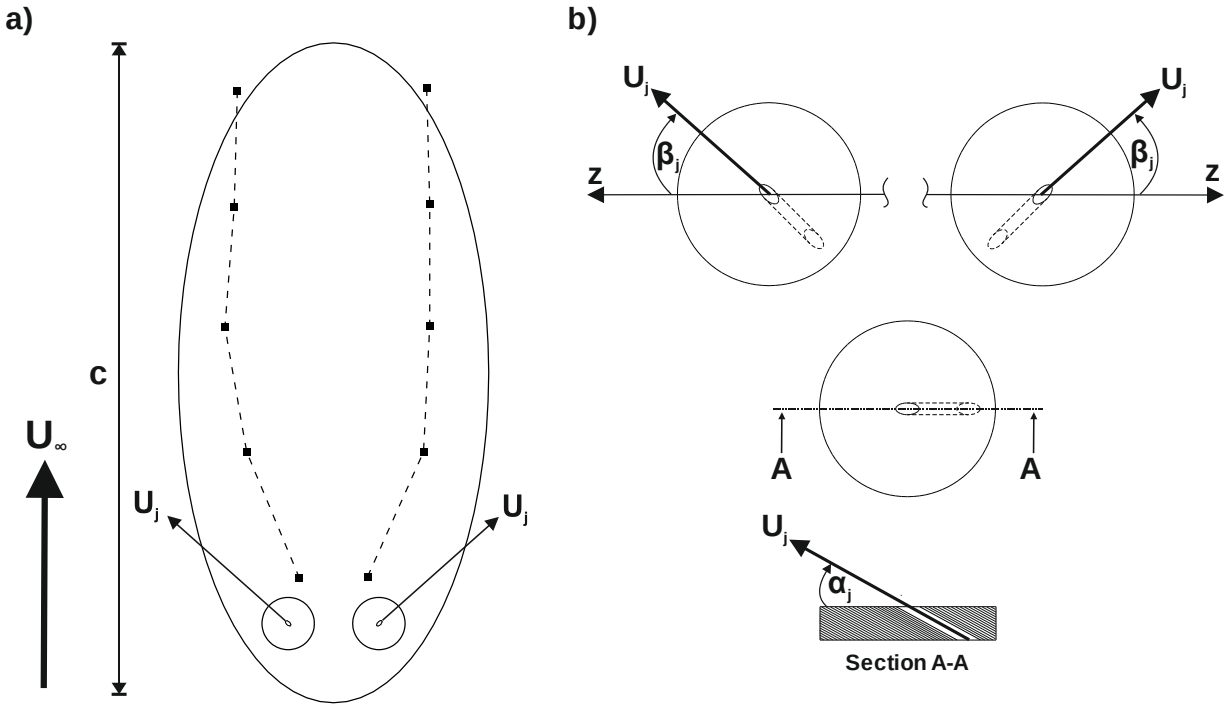


**Figure 3. Key parameters for the blowing configurations, showing a) the upswept face and the vortex trajectory for the baseline case, with one of the blowing locations ($x_j/L = 0.12$) for reference; b) the definition of yaw and incidence angles for the blowing jets.**

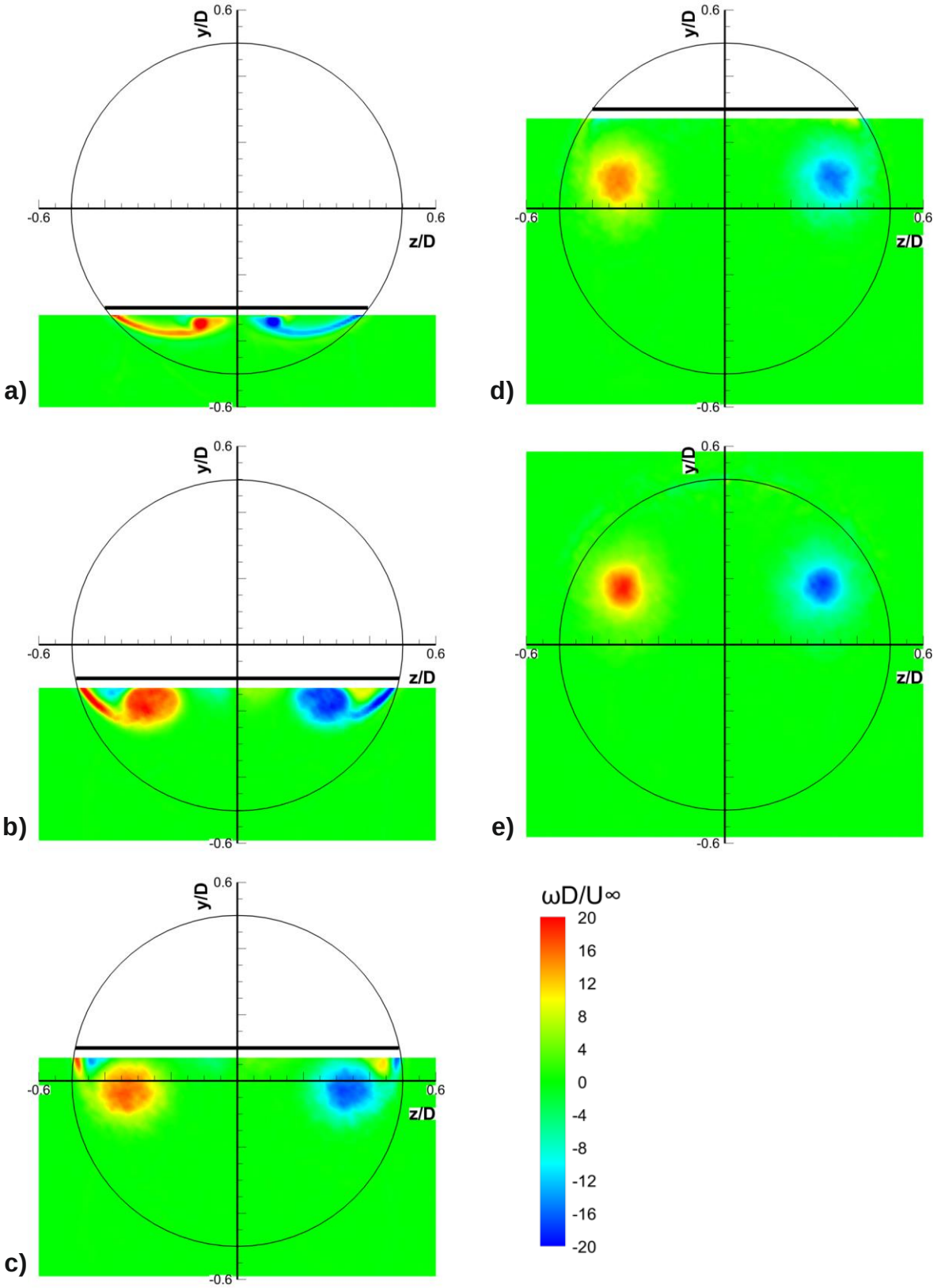


**Figure 4. Time-averaged crossflow vorticity for the baseline case at a) x/L = 0.2, b) x/L = 0.4, c) x/L = 0.6, d) x/L = 0.8 and e) x/L = 1.0. The intersection of the laser sheet with the model is marked by a thick horizontal black line.**

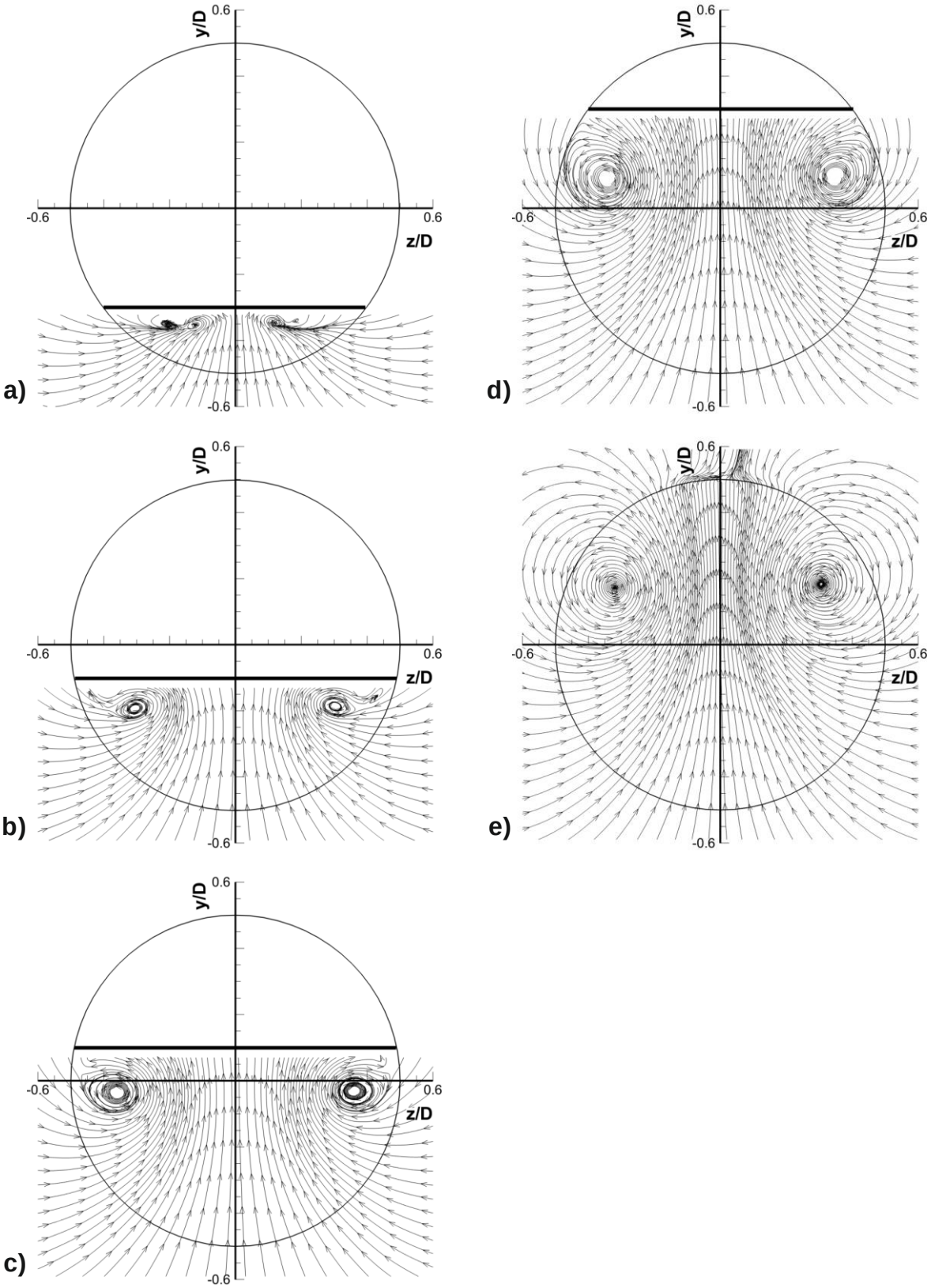


**Figure 5. Streamlines from time-averaged velocity data for the baseline case at a) x/L = 0.2, b) x/L = 0.4, c) x/L = 0.6, d) x/L = 0.8 and e) x/L = 1.0. The intersection of the laser sheet with the model is marked by a thick horizontal black line.**

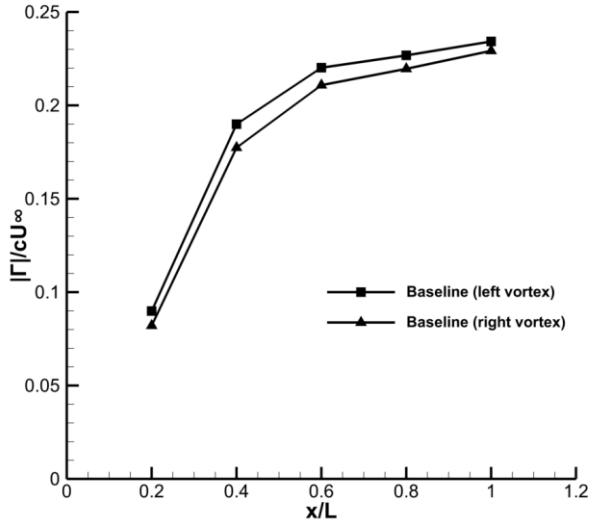


**Figure 6. Development of the vortex pair circulation with streamwise distance for the baseline case.**

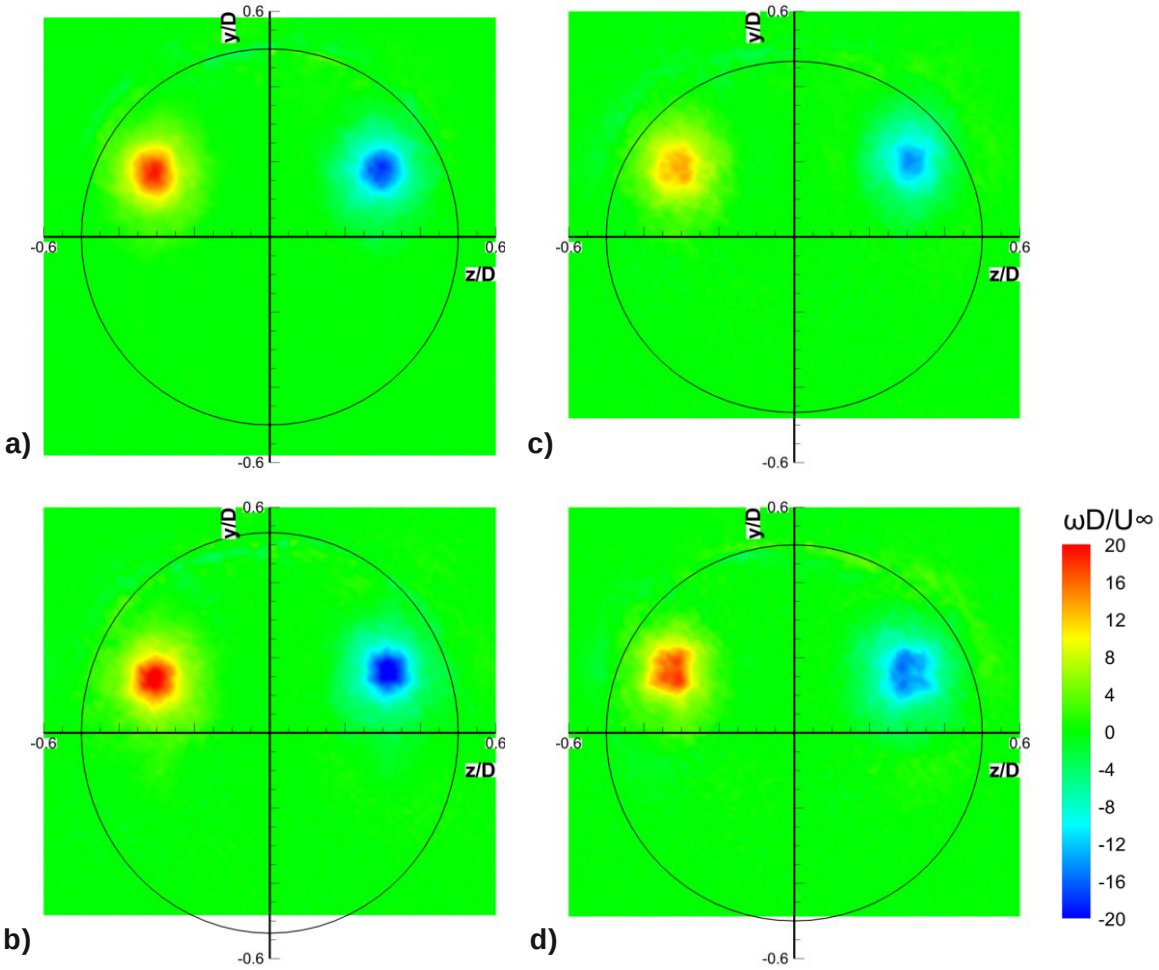


**Figure 7. Effect of a non-zero fuselage pitch or yaw angle upon the time-averaged vorticity at x/L = 1.0. Configurations are: a) baseline, b) α = -2°, c) α = +2° d) β = +2°. Camera position is unchanged between configurations. Outline of model is shown as seen from camera view.**

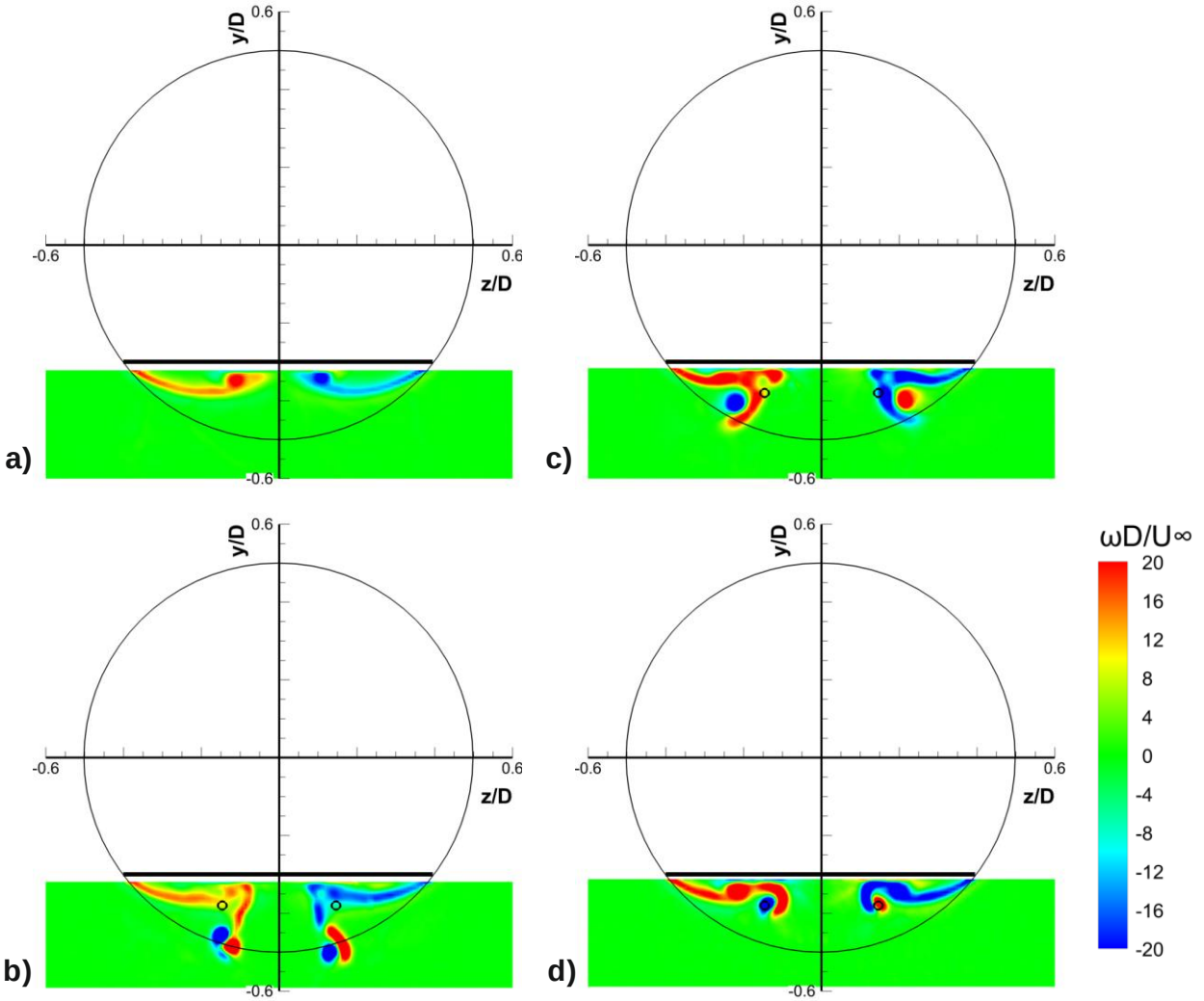


**Figure 8. Time-averaged vorticity when blowing at a streamwise location of $x_j/L$ = 0.12. Jet positions are indicated by small black circles. Measurement plane is fixed at x/L = 0.2. Configurations are: a) baseline; b) $\alpha_j = 90°$; c) $\alpha_j = 30°$, $\beta_j = 0°$; d) $\alpha_j = 30°$, $\beta_j = 90°$.**

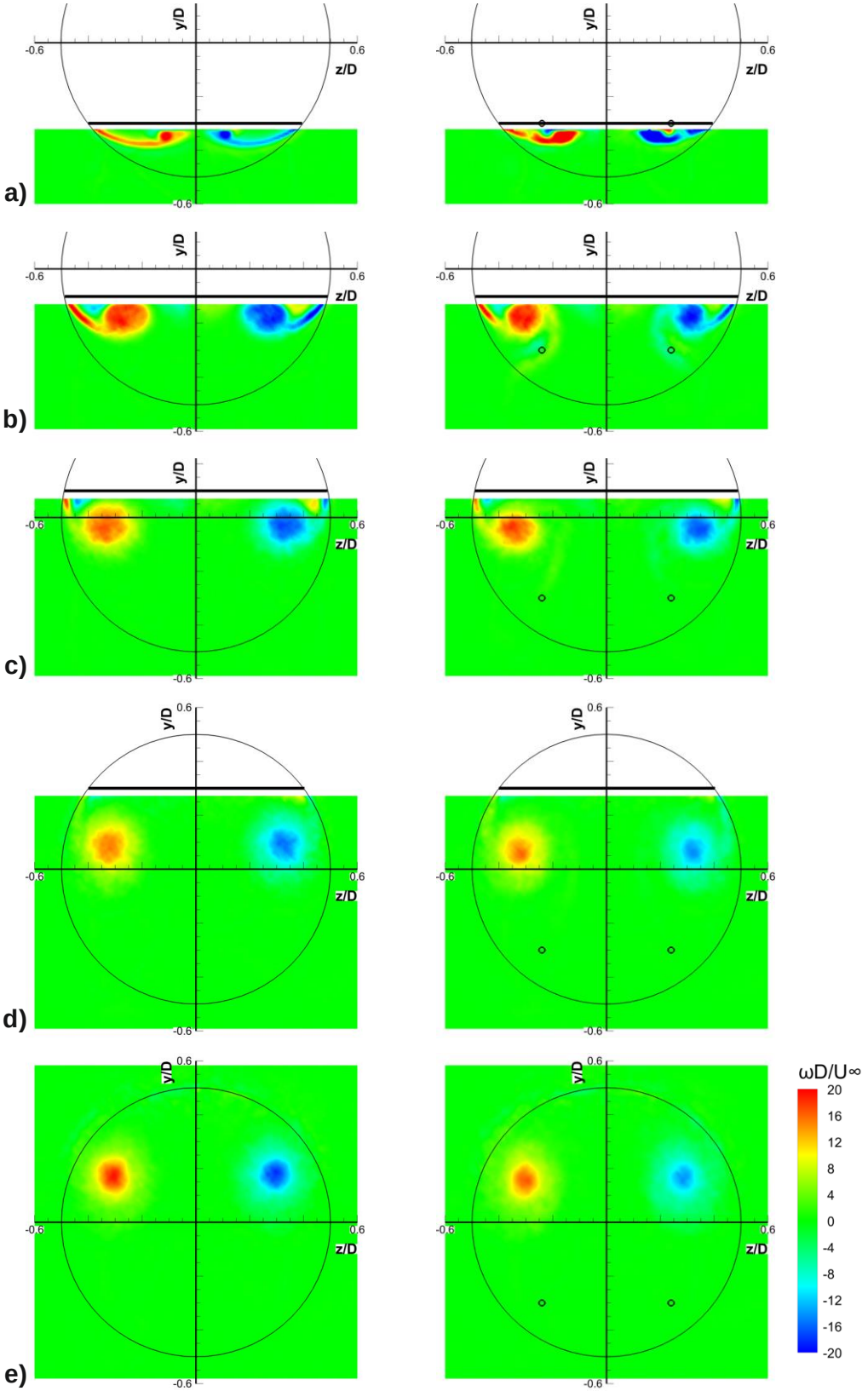


**Figure 9. Time-averaged crossflow vorticity of the baseline case, left, and one blowing configuration ($x_j/L$ = 0.2, $\alpha_j = 30°$, $\beta_j = 0°$), right. Jet positions are indicated by small black circles. Measurement planes are located at a) x/L = 0.2, b) x/L = 0.4, c) x/L = 0.6, d) x/L = 0.8 and e) x/L = 1.0.**

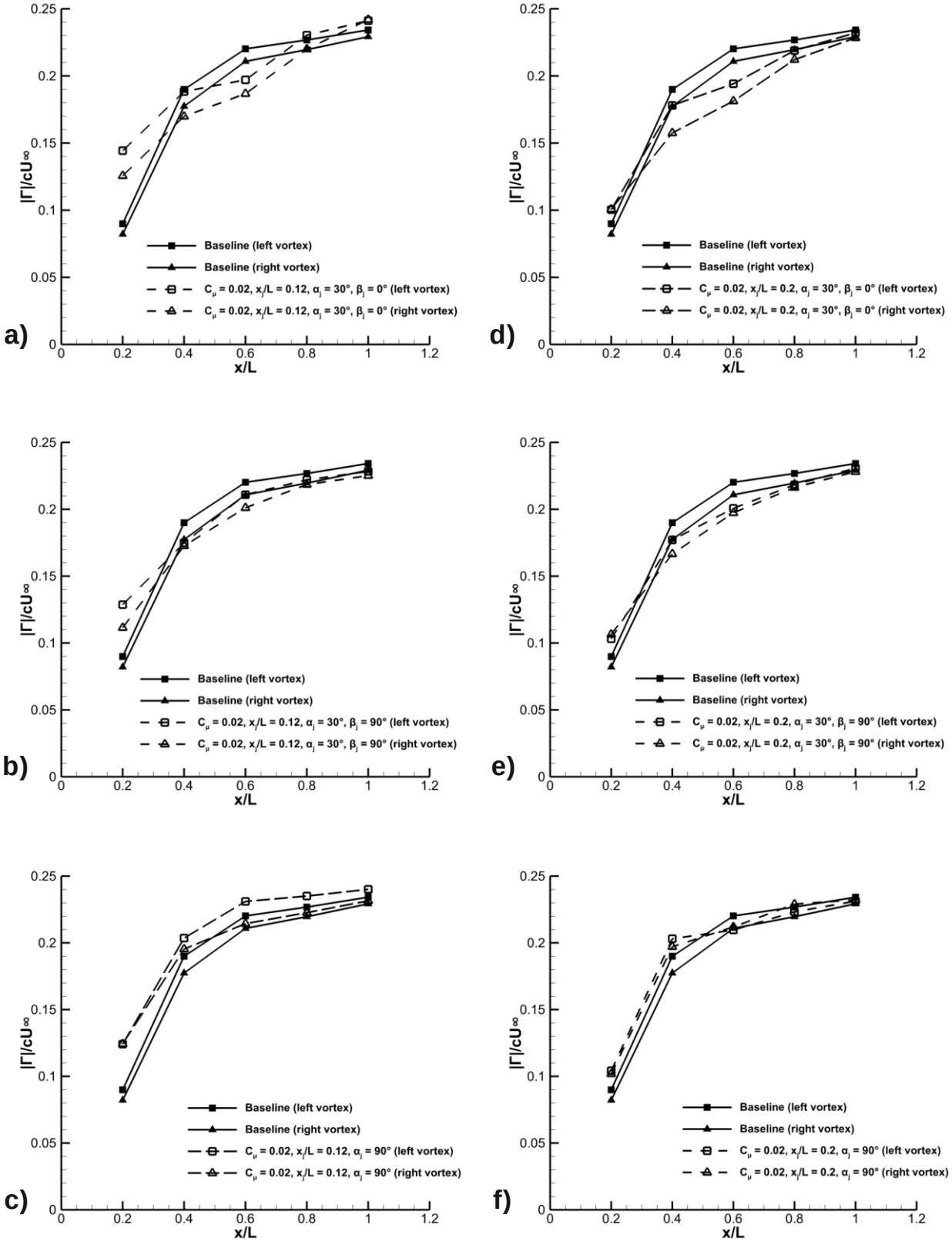


**Figure 10. Development of the crossflow vortex circulation with streamwise distance for the different blowing configurations: a) through to c) $x_j/L = 0.12$; d) through to f) $x_j/L = 0.2$.**

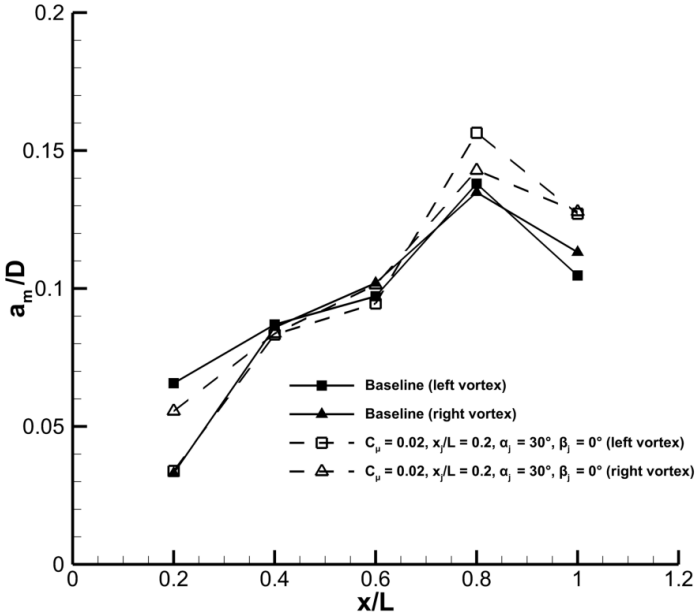


**Figure 11. Variation of vortex meandering with streamwise distance for the baseline case and when blowing at $x_j/L = 0.2$, $\alpha_j = 30°$, $\beta_j = 0°$.**

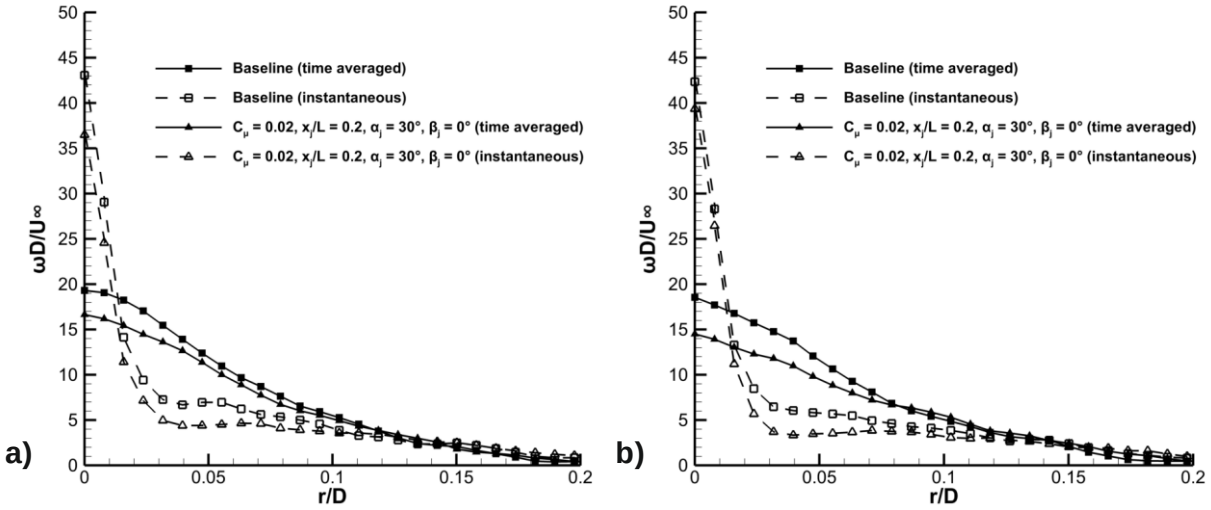


**Figure 12. Crossflow vorticity of a) left and b) right vortices at x/L = 1.0 for the baseline case and when blowing at $x_j/L = 0.2$, $\alpha_j = 30°$, $\beta_j = 0°$.**